Hierarchical Variable Fidelity Methods for Rotorcraft Aerodynamic Design and Analysis

Eliot W. Quon Marilyn J. Smith
Daniel Guggenheim School of Aerospace Engineering
Georgia Institute of Technology
Atlanta, Georgia 30332

Glen R. Whitehouse Daniel A. Wachspress
Continuum Dynamics, Inc.
Ewing, New Jersey, 08618

A coupling framework has been developed for unstructured computational fluid dynamics (CFD) solvers to allow for simple activation of a variety of wake solvers. In addition, the interface has been parallelized and extended to support dynamic, overset meshes in rotating frames. Wake capture and performance calculations demonstrate the validity of the framework. Demonstration cases include an oscillating wing, the hovering Caradonna-Tung rotor and ROBIN rotor-fuselage interaction for multiple coupling variations between CHARM, VorTran-M, and FUN3D. These results illustrate that the hybrid methods can provide more accurate results with reduced grid sizes for various applications. The modification of only one solver at each incremental level of analysis permits the user to identify the source of changes in solution results.

Background

Lifting bodies produce wakes that interact with other bodies immersed in the same fluid. In particular for rotorcraft, the problem becomes significantly more complicated since the rotor wake remains near the vehicle in hover, ascent and low-speed forward flight. The proximity of the wake increases induced inflow and reduces helicopter thrust. Moreover, since the main rotor wake may impinge on the fuselage, such interactions are an important consideration in modern rotorcraft design. For example, empennage impingement may result in undesirable handling qualities such as low-speed pitch up and tail buffet. Moreover, the wake can also generate unsteady impulsive loads on the fuselage, resulting in vibrations, thus negatively impacting the crew and passenger flight experience. Given the complexity of rotorcraft interactional aerodynamics problem, it is common for tail and empennage designs to be modified significantly after first flight (Ref. 1).

Development of many aerospace technologies, not limited to helicopter rotor-fuselage applications, requires accurate resolution of both near- and far-field flow phenomena. In rotorcraft, far-field resolution is especially important due to the persistence of wakes for long periods of time. However, numerical predictions involve a trade-off between accuracy, turn-around time and computational expense (Ref. 2). Current grid-based CFD codes can theoretically model the entire flow field, but resolution and preservation of wake features becomes difficult since typical grid sizes used in industrial simulations are susceptible to numerical dissipation. The artificial diffusion of vorticity that results can be mitigated using grid adaptation techniques and higher-order methods (Refs. 2–4), but this may not be practical for all applications since computational cost increases significantly. For this reason, computationally efficient hybrid methods may be more attractive, especially during design and for flight test support.

Traditional Lagrangian free wake methods are inexpensive, but become less accurate when vortex elements in the wake become distorted and tangled due to interactions with other vortices and solid bodies (i.e. rotor blades and the fuselage) (Ref. 5). These interactions typically occur in the rotor near field (e.g. BVI), which motivates coupling to a CFD solver to resolve the highly viscous and possibly compressible flow near the rotor. In such an approach, the CFD code does not have to resolve the entire wake region, thus the size of the CFD domain can be greatly reduced and computational efficiency maximized. Several hybrid CFD/free-wake methods have been previously developed; however, while predictions of the normal forces have been generally improved, pitching moments have been less well captured (Ref. 6). Additional challenges associated with

Presented at the American Helicopter Society 67th Annual Forum, Virginia Beach, VA, May 3-5, 2011.

surface interactions arise when modeling problems such as ship-wake interactions and vehicle-ground interactions. Using a vorticity-velocity CFD solver to evolve the wake directly addresses many of these issues, though at increased computational cost. Nevertheless, in order to obtain the best wake representation, it is essential to capture the effects of viscosity and compressibility in the rotor near field using a conventional CFD approach. As with a free-wake coupled methodology, the physical extent of the CFD domain can be minimized, thus reducing the overall cost when compared to pure CFD calculations (Ref. 5).

The ability to interchange one component of the near- or far-field simulation model, while maintaining the other components lends itself to the ability to consistently assess the simulation quality at different levels of fidelity. Thus, a collection of computational methods in a single framework allows for straightforward variation from initial design to detailed analysis at decreased time and cost, as illustrated in Fig. 1. This paper presents such a hierarchy of CFD-based hybrid methods, comprising an aerodynamics module derived from a comprehensive rotorcraft analysis code (Ref. 7), a vorticity-velocity CFD solver (Ref. 8) and a primitive-variable RANS CFD approach (Ref. 9). Validation of the hybrid methods (FUN3D/CHARM and FUN3D/VorTran-M) are shown, along with two rotorcraft applications of interest: a rotor in hover and rotor-fuselage interactions.

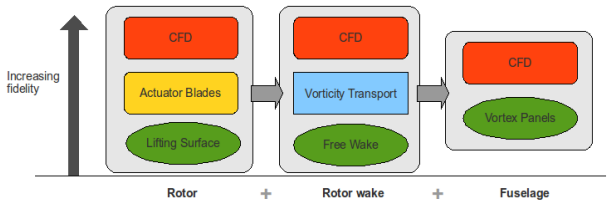

Fig. 1: Combinations of three different codes for increasing levels of fidelity.

Computational Methodologies

Continuum Dynamics Inc.'s (CDI) comprehensive rotorcraft code, CHARM, has been used successfully to model rotorcraft airloads and BVI noise (Ref. 10). CHARM is equipped with lifting surface blade aerodynamics and a full-span free-vortex wake model, and uses no empirical parameters to model the roll-up of the wake sheet into concentrated vortices. The free wake model does not dissipate vorticity and offers real-time turnaround (Ref. 7). Surface pressures can be determined with an integrated panel method (Ref. 11).

A higher fidelity wake solution can be obtained using CDI's VorTran-M module. VorTran-M solves the incompressible Navier-Stokes equations in vorticity-velocity form on an adaptive Cartesian grid. This approach, which explicitly conserves vorticity, has been effective at predicting rotor wakes over many revolutions when coupled to a variety of near-body solvers (Ref. 8). Recently, VorTran-M has been coupled to several Cartesian, structured, and unstructured CFD codes (Ref. 5), including the solver demonstrated in this effort.

The CFD code chosen to demonstrate the coupling is FUN3D (Ref. 9), a fully unstructured Navier-Stokes RANS solver developed primarily by researchers at NASA LaRC and Georgia Institute of Technology. This code has overset and adaptive mesh capabilities to enable accurate resolution of multiple frames of motion, making it suitable for rotorcraft analysis. In addition, FUN3D include a number of source-based rotor models, including actuator blades (Refs. 12, 13), which are a viable alternative to lifting surface aerodynamics. Actuator blades can provide geometric degrees of freedom along the chord and radius, and it can model model non-linear twist distributions. Moreover, the actuator sources provide additional flexibility in modeling the pressure jump across the rotor at negligible cost compared to full-blade CFD.

An interface between FUN3D and CHARM or VorTran-M has been developed to perform fully-coupled time-accurate calculations. The FUN3D near-body solution is used to determine the local flow field at each time step, which is inserted into the VorTran-M domain as velocity at the cell corners of appropriate VorTran-M cells. Alternatively, an equivalent blade loading or bound vortex can be determined for the CHARM module to update the strength of vortex filaments. After the wake solution is advanced, induced velocities are calculated and their influence is imposed on the outer boundary of the FUN3D domain through a modified far-field boundary condition. The FUN3D solution is then advanced to the next time step and the coupling cycle repeats.

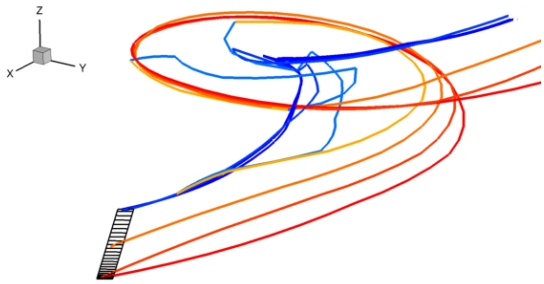

Fig. 2: Fully coupled FUN3D/CHARM simulation of a single rotating UH-60 rotor blade in high-speed forward flight. The rotor is advancing in the $+x$ direction.

Background grid	Fully coupled w/ VorTran-M	Total # of Cells	C_L	Error (%)
none	no	270k	0.7732	7.9
farfield $\rightarrow 5c$	no	4.4M	0.7616	6.3
none	yes	420k	0.7326	2.2
-	-	-	0.7166	0.0

Table 1: FUN3D predicted lift for NACA0012 wing at $\alpha = 8^\circ$, compared with experimental data from (Ref. 14).

Hybrid Methodology Validation

FUN3D + CHARM

The FUN3D/CHARM coupling interface was developed specifically for rotorcraft applications. To validate the coupling, a case similar to the UH-60 8534 case (high-speed forward flight, $\mu = 0.368$) was run using a single rotor blade in FUN3D. Blade loadings were passed from FUN3D to CHARM, and induced velocities passed from CHARM to FUN3D. Roll-up of the CHARM vortex trailers was observed in the wake (Fig. 2), where vortex strengths were calculated from the FUN3D blade loadings.

FUN3D + VorTran-M

To validate the FUN3D coupling with VorTran-M, basic test cases with a NACA0012 wing and finite cylinder (with aspect ratios of 8.8 and 4.0, respectively) were run in a non-rotating frame. Using a free stream Mach number of 0.2 and the incompressible path within FUN3D, the wing was simulated at 8° angle of attack. A 240,000 node tetrahedral mesh that extended one chord length beyond the wing in all directions was used for these simulations. To provide data for correlation, the two-dimensional lift curve slope (a_{2D}) from Abbott and von Doenhoff (Ref. 14) (6.3025/rad) was modified to account for three-dimensional effects using the well-known aspect ratio correction (Ref. 15). Table 1 illustrates that a notable improvement in the predicted lift is observed when coupled to VorTran-M, using an order of magnitude fewer cells than the FUN3D simulation alone.

A dynamic case was then evaluated with the wing pitching at $8\pm5^\circ$ at a reduced frequency of $k = \omega c/2U_\infty = 0.5$. The run successfully demonstrates dynamic update of the overset insertion region in which the flow field is passed from FUN3D to VorTran-M (Fig. 3). The VorTran-M domain is dynamically resized to encompass the convected vorticity that remains purely outside the FUN3D domain. Again, preservation of shed vorticity including the starting vortex was observed. In addition, the corresponding VorTran-M solution shows three-dimensional wake development (Fig. 4). In particular, the pitching moment shows excellent correlation, matching both magnitude and phase, while the lift shows a slight magnitude reduction and phase delay due to the increased wake influence.

The classical problem of a circular cylinder in a cross-flow was evaluated both in terms of predicted Strouhal number and the wake structure. A free stream Mach number of 0.2 with a Reynolds number of 3900 was investigated. The fully tetrahedral grid consisted of 3 million nodes, which is larger than the prior grids, but which acted as a verification of the capability of the parallel hybrid computations. It should be noted that Lynch (Ref. 12) found that the tetrahedral grid was not the best for this problem; a mixed-element mesh with specified boundary layer aspect ratio cell sizes and growth was required to capture the most accurate surface characteristics. The FUN3D-alone grid spanned 19.5 diameters downstream, while the near-body FUN3D/VorTran-M grid spanned 3.5 diameters in the wake. The predicted primary Strouhal number for the FUN3D/VorTran-M simulation was extracted at the midspan and computed to be 0.20, matching the experimental and FUN3D simulation predictions (Ref. 12) on the full grid. When running the near-body grid with coupling, significant three-dimensional flows are observed (Fig. 5), as is expected from the configuration.

Accuracy of Wake Geometry for a Rotor in Hover

The two-bladed hovering rotor of Caradonna and Tung (Refs. 16, 17) provides an excellent correlation case with which to evaluate the FUN3D/VorTran-M methodology. The experiments included numerous blade pressure and tip vortex geometry measurements, and have shown that both the blade loadings and vortex trajectories are relatively insensitive to rotor tip speed (Ref. 16). For this study, the rotor was run at 1250 RPM ($M_{tip} = 0.439$) with a fixed collective pitch of 8°.

The rotor was simulated via an overset grid arrangement where only a single blade was directly modeled in FUN3D. Given the symmetry in the loading of the hover scenarios, the predicted flow field that initializes the VorTran-M vorticity distribution can be duplicated, rotated by 180 degrees, and inserted as the second blade (Fig. 6). The advantage of this approach is that the cost of the calculation can be reduced through the reduction of mesh nodes (as only one blade is modeled), while still retaining the full unsteady influence of two blades on the rotor wake.

A series of snapshots of the rotor wake (Fig. 7) illustrates the capture of the blade-vortex interaction that is

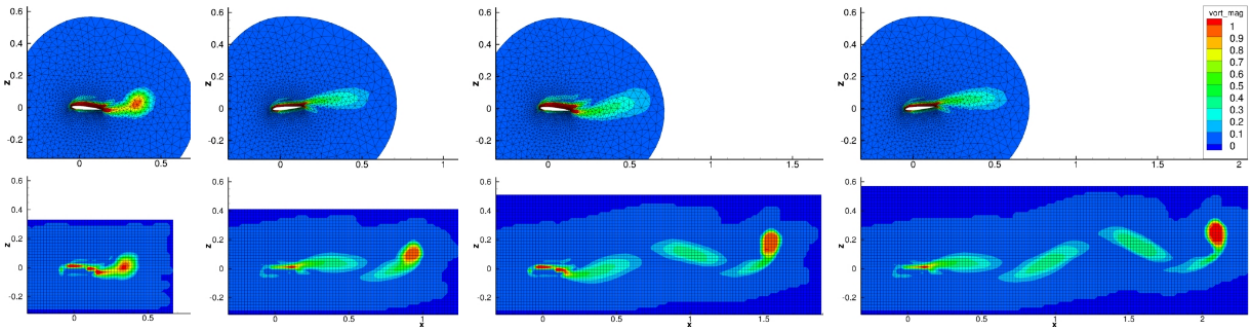

Fig. 3: Vorticity magnitude of a pitching NACA0012 wing with FUN3D/VorTran-M coupling, showing the coupled wake evolution after 1-4 vortex shedding cycles. The top row shows the flowfield output from FUN3D and the bottom row shows the corresponding flowfield from VorTran-M.

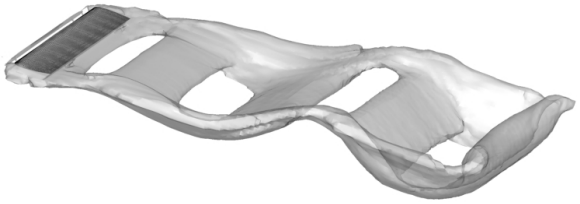

Fig. 4: Iso-surfaces of vorticity magnitude for pitching NACA0012 wing.

present, and demonstrates the build-up of the wake structure as VorTran-M captures the long-age wake in hover. The characteristic of the resulting flow field can be observed via vorticity in Fig. 8.

Sectional lift (averaged over one rotor partial-revolution) compares favorably with experiment (Fig. 10). In the coupled FUN3D/VorTran-M case the average error compared to experiment is less than 10% and represents a drastic improvement over the standalone FUN3D case. Lift is slightly under predicted on the inboard portion of the blade, as a result of vortices persisting near the blade root. Similar flow features were also observed in calculations using the structured CFD solver, OVERFLOW (Ref. 5). Alternative techniques such as adaptive mesh refinement are expected to improve the inflow prediction in this region. Corresponding pressure distributions at select radial stations are shown in Fig. 9 and demonstrate the same reduction in inboard blade loading. In all cases, the coupled result predicts pressures closer to the experimental values. Significant improvements are observed near the tip using FUN3D/VorTran-M coupling, with the experimental location and amplitude of the suction peak being accurately captured at the two furthest outboard stations.

The grid used in the FUN3D/VorTran-M coupling contained 2.2 million nodes, reduced from 5.3 million nodes in the FUN3D standalone case. Additional improvement may be obtained with the feature-based adaptation demonstrated in Ref. 4 to focus grid nodes where they are needed for both applications of FUN3D. It is anticipated that, in

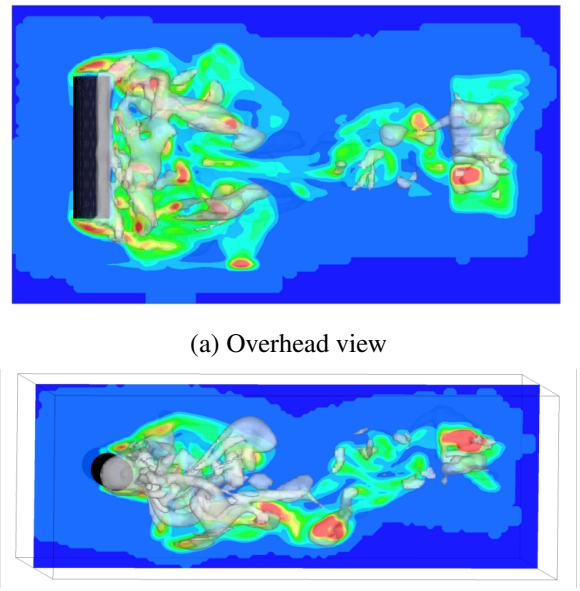

(a) Overhead view

(b) Side view

Fig. 5: Iso-surfaces of vorticity magnitude for finite cylinder in crossflow, with vorticity contours shown in the mid-span plane.

order for FUN3D to produce loads of the same accuracy as the coupled case, significant grid refinement in the wake region will be necessary, thus corresponding to increased computational expense.

Rotor-Fuselage Interactions

Rotor-fuselage interactions were investigated by Mineck and coworkers at NASA Langley Research Center using a generic fuselage configuration (the ROtor Body INteraction, or ROBIN, model) (Refs. 18–20). The ROBIN fuselage geometry is defined by a set of algebraic equations at various fuselage stations to yield a streamlined slender fuselage body and an engine mount (doghouse). Wind tunnel tests were performed with and without a 4-bladed rectan-

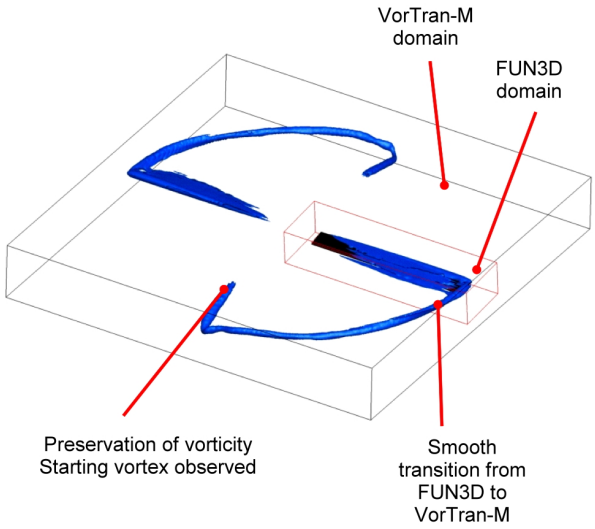

Fig. 6: Schematic of FUN3D/VorTran-M grid arrangement for the two bladed rotor in hover.

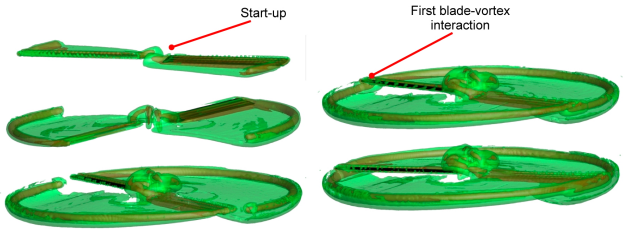

Fig. 7: Snapshots of the hovering rotor wake predicted by FUN3D/VorTran-M.

gular rotor with solidity, $\sigma = 0.098$. The 33.88 inch blades were comprised of a NACA 0012 section with a 2.7 inch chord and -8° linear twist. The tests are summarized in the recent paper by Smith et al. (Ref. 21), including data corrections and trim conditions for FUN3D.

The steady and unsteady loading on the ROBIN fuselage was investigated using CHARM and the coupled FUN3D/CHARM. Predictions are compared to experimental data (Refs. 18–20), as well as prior numerical predictions made with FUN3D and VTM (i.e. a precursor to VorTran-M coupled to lifting line blade aerodynamics and a non-lifting panel method)) (Refs. 21–25).

Isolated Fuselage

CHARM predictions of the isolated fuselage using 2174 panels are compared to the experimental data (Ref. 20), FUN3D (Ref. 21) and VTM calculations (Ref. 23) in Fig. 11. All three sets of predictions are generally very good up to 18% of the fuselage length ($x/\ell = 0.35$). At $x/\ell = 0.47$ and locations aft, CHARM and FUN3D predict pressures that vary little around the fuselage, as one would expect for the non-lifting streamlined symmetrical body. At $x/\ell = 0.47$, there is flow separation at $z/\ell > 0.1$

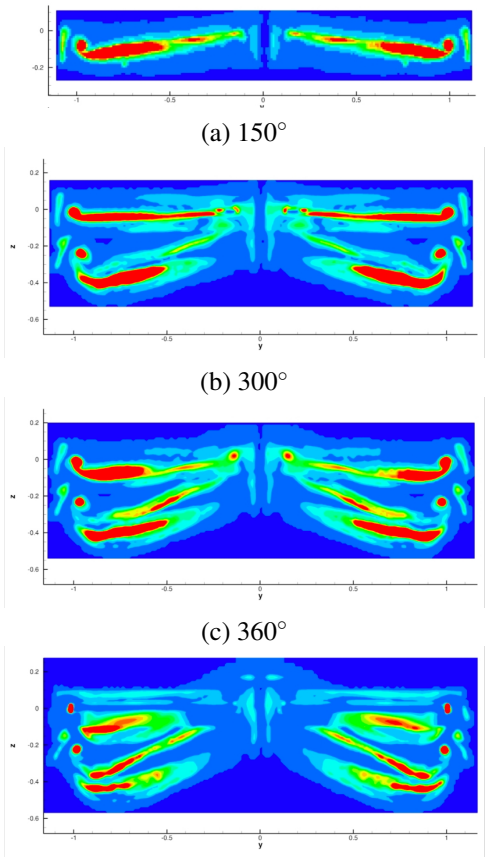

(a) 150°

(b) 300°

(c) 360°

(d) 450°

Fig. 8: Illustration of the temporally developing wake of a hovering rotor (wind turbine at zero yaw) captured by FUN3D/VorTran-M. The vorticity magnitude illustrates the crispness of the vortex sheet and tip vortex as it moves away from the rotor blade.

predicted by FUN3D, which as expected from inviscid theory, is not predicted by CHARM. The reason why the VTM panel method predicts a separation-like trend is not currently known.

Standalone Code Calculations of the Unsteady Pressure

Unsteady pressure predictions along the top of the fuselage at $x/\ell = 0.2$, 0.9, 1.18 and 1.56 are presented in Figs. 12 and 13 for advance ratios of $\mu = 0.15$ and 0.23. Unless otherwise stated, CHARM predictions were performed with 24 azimuthal increments, 16 spanwise filaments and a total of 7 turns of wake (3 turns of full-span followed by 4 turns of tip and root filaments). Calculations were trimmed for 20 revolutions. With the controls held fixed, each calculation was run for an additional 20 revolutions, over which the predicted pressures were averaged.

Overall, it is seen that the CHARM predictions are consistent with previous predictions made with VTM and FUN3D (Refs. 21–25) though at a fraction of the computa-

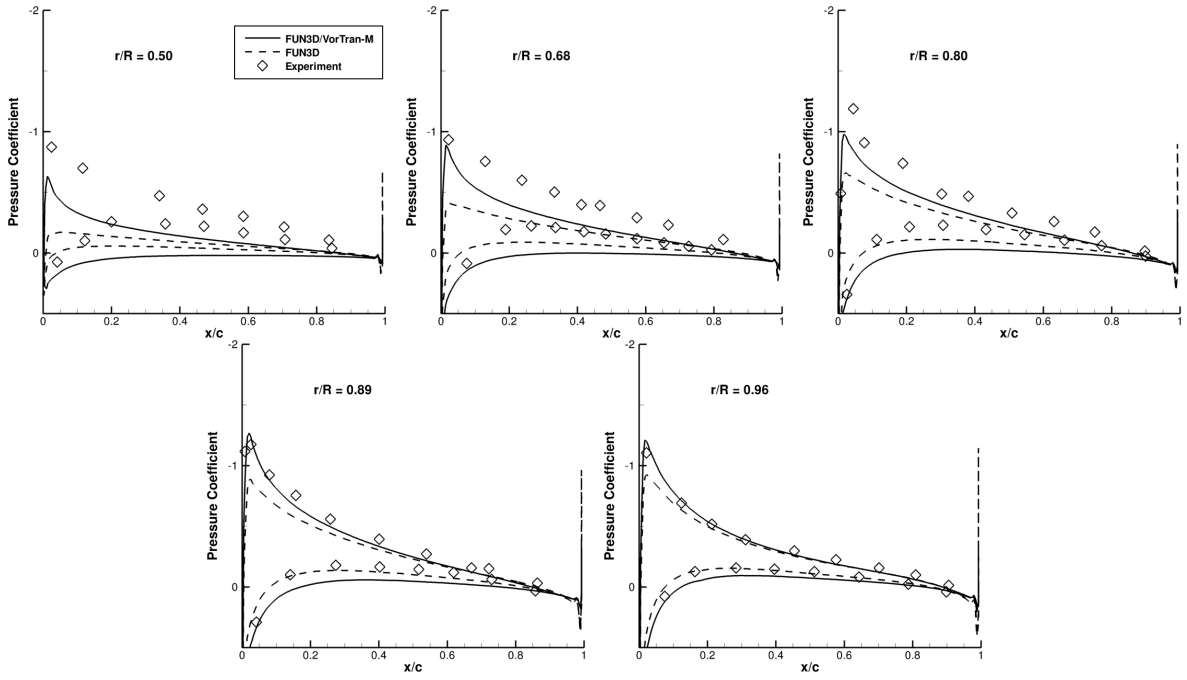

Fig. 9: Pressure distributions for the Caradonna-Tung rotor at various radial stations.

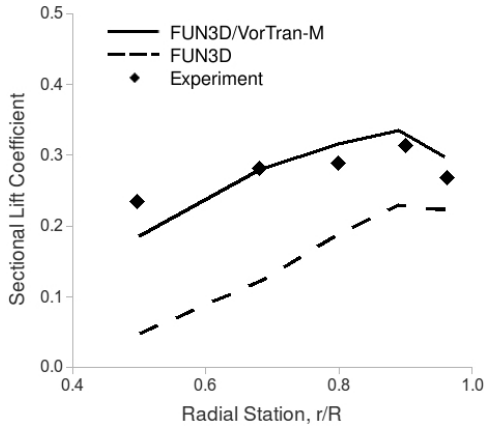

Fig. 10: Blade span loading for the Caradonna-Tung rotor.

tional cost. All three analyses closely match the experimental data in areas where viscous effects can be neglected. At $\mu = 0.15$ (Fig. 12), CHARM, VTM and FUN3D all match the data well in terms of both phase and magnitude except for a slight under prediction of magnitude at $x/\ell = 1.18$. It is believed that this discrepancy is due to bluff body shedding off the aft end of the doghouse and hub on the top of the fuselage (Ref. 23). A similar trend is observed at $\mu = 0.23$ (Fig. 13) where predictions fore and aft of the doghouse are generally excellent but all three analyses significantly under predict the magnitude of the pressure pulses along the top of the doghouse.

Figure 14 shows predictions along the sides of the doghouse, however these predictions are mixed. All three analyses capture the phasing well on the advancing side, though the amplitude is under predicted. On the retreating side, the trends are reversed, with the analyses generally predicting the amplitude, but not the phase. In general, all three analyses are in close agreement.

Hybrid FUN3D/CHARM Calculations of the Unsteady Pressure

Two different types of interactional aerodynamics test calculations were undertaken to demonstrate the hierarchical variable fidelity approach. Firstly a coupled FUN3D/CHARM prediction of the ROBIN configuration at $\mu = 0.15$ was undertaken where FUN3D was used to predict the blade airloads, and the CHARM wake panel module was used to predict the rotor wake and the fuselage. Then a calculation of the ROBIN configuration again at $\mu = 0.15$ was undertaken where CHARM predicted the blade airloads and rotor wake, whereas FUN3D was used to predict the unsteady fuselage loading.

FUN3D Rotor Blades and CHARM Wake and Fuselage: FUN3D and the CHARM wake panel module were coupled together in a "conventional" hybrid arrangement where FUN3D was used to predict the blade airloads and the CHARM wake panel module was used to predict the rotor wake. In a first, to our knowledge, for this type of hybrid arrangement, a fuselage was included in the calculation using CHARM's integrated panel model. The ROBIN blade grids used in these studies contained 9.2 million nodes (4

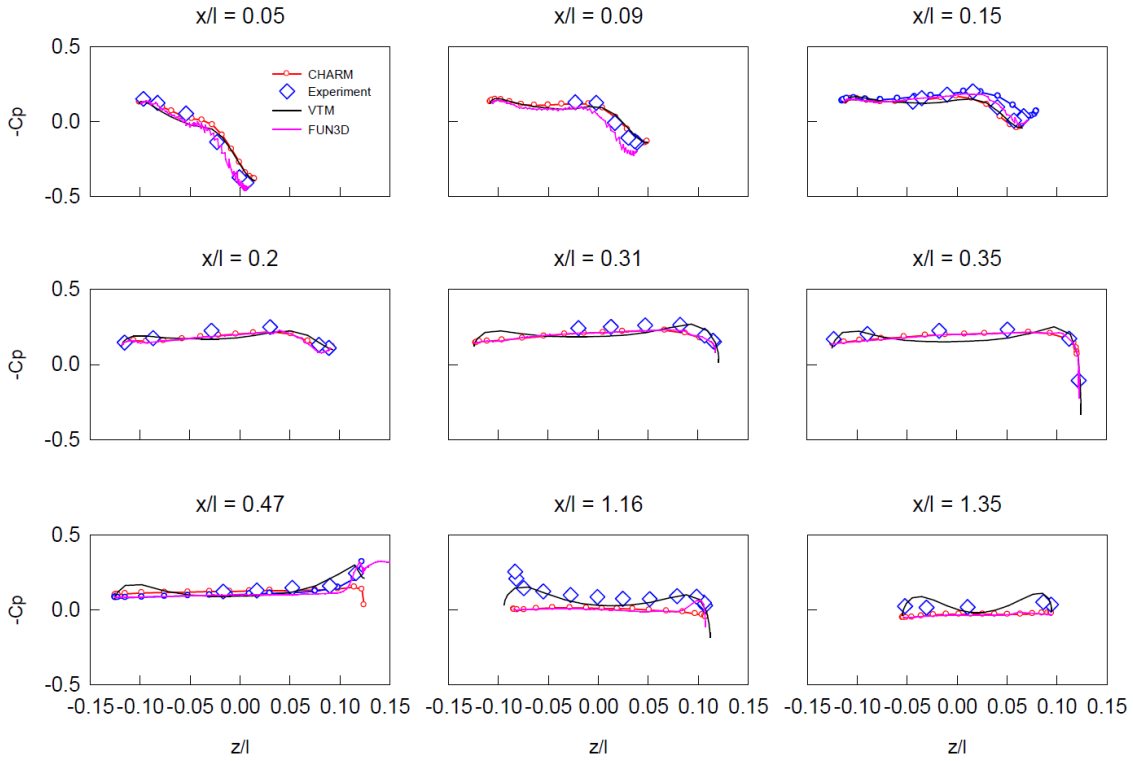

Fig. 11: Pressure on the isolated ROBIN fuselage at various locations.

blades with near field grids of 2.31 million points each from (Ref. 21). In order to model the cyclic motion present in the simulation, a small background grid was generated. Coupled calculations were run for FUN3D, FUN3D/CHARM and CHARM predictions for $\mu = 0.15$ and $C_T = 0.0064$ are compared with experimental data in Fig. 15. In general, all predictions show good reproduction of the magnitude and phase of the peaks in unsteady pressure, though none predict the peak magnitude downstream of the doghouse where separation and hub (not modeled here) effects may be significant. The impact of the FUN3D/CHARM computations can be readily observed at this moderate advance ratio. Just below the hub ($x/\ell = 0.9$) the predicted pressures differ the most due to a large unsteady separated flow in this area. Compression peaks predicted by FUN3D/CHARM are close to the high resolution FUN3D predictions, but the suction peaks are closer to the CHARM solutions. The closer approximation at the compression peaks is due to the difference in the rotor wake prediction by FUN3D. On the aft fuselage at $x/\ell = 1.18$, a wake/fuselage interaction was observed in pure FUN3D predictions (Ref. 21), the FUN3D/CHARM results provide the best correlation with experiment, which suggests the potential of the hybrid methodology. Similar improved correlations can be seen at $x/\ell = 1.56$, although the suction peaks tend to be over predicted. The coupled FUN3D/CHARM more accurately predicts the slopes of the pressures and appears to capture the higher harmonic feature in the unsteady pressures at about 110°. However, similar features at 200° and 290° are not well captured by any of the three methods. Nevertheless, given the significant reduction in computational costs (18 hours per rev on 64 processors for pure FUN3D verses 9.6 hours per revolution for the coupled FUN3D/CHARM), results are very promising.

The complex FUN3D/CHARM wake structure for the $\mu = 0.15$ case is shown in Fig. 16, where the interaction of the wake with the aft empennage is clearly apparent. In Fig. 16, the wake is colored by release location along the blade; blue vectors are also shown in these figures and represent the wake induced velocity at each of the FUN3D nodes along the boundary.

FUN3D Fuselage and CHARM Rotor Blades and Wake: To demonstrate the potential of the variable fidelity hybrid arrangement, FUN3D and CHARM were coupled together where a CHARM rotor and wake would interface with a viscous FUN3D fuselage. Rotor airloads were calculated with CHARM at 1 degree increments, and the wake set the outer boundary conditions on the FUN3D domain. The FUN3D ROBIN fuselage grid (Fig. 13) was comprised of 4.3 million cells with outer extents of three fuselage lengths in the free stream velocity direction, 0.5 lengths in width and 1 length in height, with the fuselage placed near the top of the grid such that the rotor disk plane was just above the upper domain boundary.

Wake predictions for this case are shown in Figs. 18 through 20 and clearly show the rotor wake descending be-

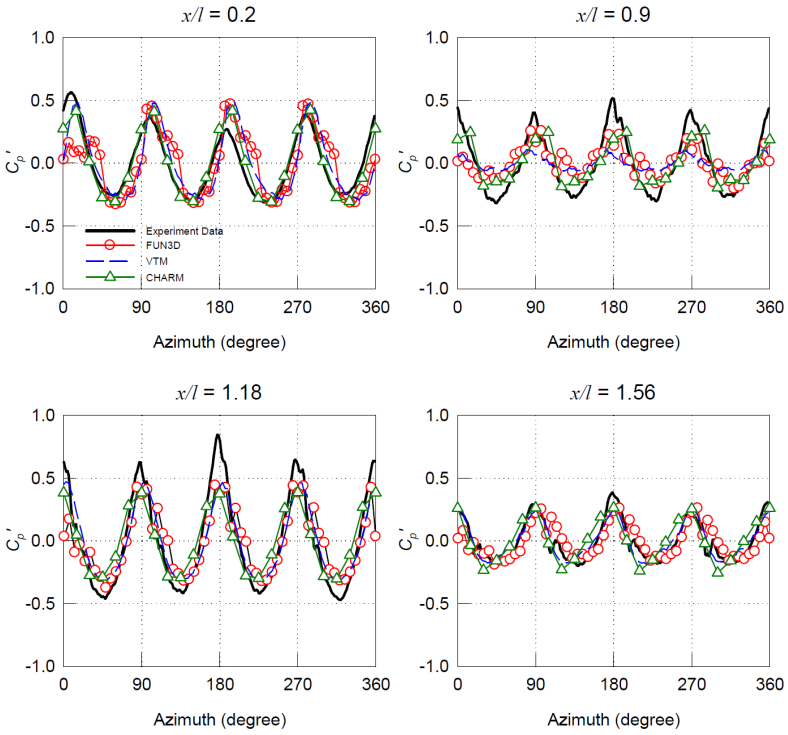

Fig. 12: Unsteady pressure at various points along the top centerline of the fuselage ($\mu = 0.15$, $C_T = 0.0064$).

low the rotor disk plane and entering FUN3D prior to impacting the aft fuselage. Complicated roll-up dynamics are observed near to the leading edge of the rotor in Figs. 18 and 19 where the tip vortices descend below the rotor disk and enter the FUN3D domain, prior to completing roll-up and convecting upwards to pass over the advancing blade. Aft of the rotor disk, the wake from each blade rolls up to form the super-vortices, as illustrated in Fig. 18. On the retreating side of the rotor these vortices pass along the upper boundary of the FUN3D domain, with half of the structure inside FUN3D and half being represented solely by CHARM. On the advancing side of the rotor, the super-vortices enter the FUN3D domain and pass close to the trailing edge of the fuselage (Fig. 19). Figure 20 shows a contour plot of vorticity magnitude along the centerline of the fuselage, along with the 3D CHARM wake for clarification. The smooth transition of tip vortices into the FUN3D grid is clearly evident, particularly upstream of the hub. Aft of the hub, complicated wake interactions take place where the inboard rotor wake impacts the rear of the fuselage.

Unsteady pressures along the centerline of the upper fuselage are plotted in Fig. 21. In general, the magnitude of the pressure peaks is similar to the FUN3D/CHARM calculation with the CHARM fuselage; however, the negative peaks at 45° and 225° at $x/\ell = 1.6$ are better captured. At $x/\ell = 0.9$ the pressure peaks are shifted by approximately 45° from the experiment and previous predictions, and this may be caused, at least in part, by the flow separation on the port side of the fuselage shown in Figs. 19 and 20.

These results were obtained with over an order of magnitude reduction in computational costs (CHARM rotor/wake and FUN3D fuselage took 1.5 hours per revolution on 64 processors; FUN3D rotor and CHARM wake/fuselage took 9.6 hours per revolution; and the pure FUN3D solution took 18 hours per revolution) when compared to pure FUN3D.

Conclusions

This paper describes the preliminary development of a CFD-based hierarchical framework of analysis tools suitable for application to the entire rotorcraft design and analysis process. This suite of tools is based around the FUN3D unstructured RANS solver (though it could be implemented in other solvers as required) and features the CHARM blade-aero/free-wake/panel module and the VorTran-M CFD wake solver. Results are presented for a variety of relevant problems, included the first presentation, to the authors' knowledge, of hybrid CFD-based predictions of rotor-fuselage interactions. Predictions demonstrate improvements in loading predictions, as well as significant reductions in computational time.

Acknowledgments

This work was supported by Navy STTR contract N68335-09-C-0335 with guidance from technical monitors Jennifer Abras and Mark Silva and in part by US DOE STTR DE-SC0004403.

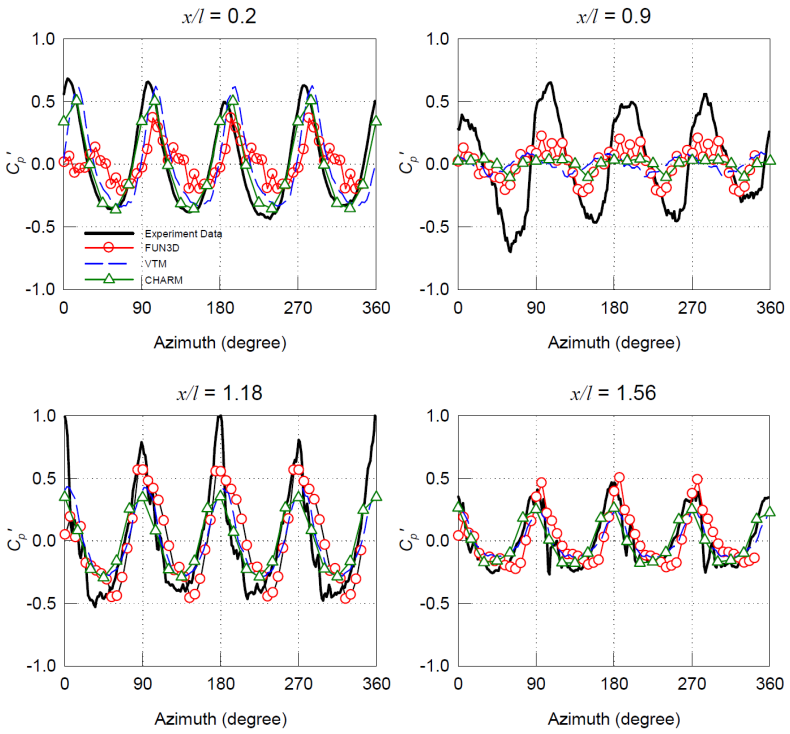

Fig. 13: Unsteady pressure at various points along the top centerline of the fuselage ($\mu = 0.23$, $C_T = 0.0064$).

References

[1]Prouty,R. W., *Military Helicopter Design Technology*, Krieger, Malabar, FL, 1998.

[2]Komerath, N., Smith, M. J., Tung, C., "A Review of Rotor Wake Physics and Modeling," *Journal of the American Helicopter Society*, to appear, 2011.

[3]Wissink, A., Potsdam, M., Sankaran, V., Sitaraman, J., Yang, Z., and Mavriplis, D. J., "A Coupled Unstructured-Adaptive Cartesian CFD Approach for Hover Prediction," *66th Annual Forum of the American Helicopter Society*, Phoenix, AZ, 2010.

[4]Shenoy, R., and Smith, M. J., "Unstructured Overset Grid Adaptation for Rotorcraft Aerodynamic Interactions," Proceedings of the 67th Annual Forum of the American Helicopter Society, Virginia Beach, VA, May 2011.

[5]Whitehouse, G. R., Boschitsch, A. H., Smith, M. J., Lynch, C. E., and Brown, R. E., "Investigation of Mixed Element Hybrid Grid-Based CFD Methods for Rotorcraft Flow Analysis," *66th Annual Forum of the American Helicopter Society*, Phoenix, AZ, 2010.

[6]*UH-60 Airloads Workshop Participant Correlations*, 2000-2010.

[7]Wachspress, D. A., Keller, J. D., Quackenbush, T. R., Whitehouse, G. R., and Yu K., "High Fidelity Rotor-Aerodynamic Module for Real-Time Flight Simulation",*64th Annual Forum of the American Helicopter Society*, Montreal, Canada, 2008.

[8]Whitehouse, G. R., Boschitsch, A. H., Quackenbush, T. R., Wachspress, D. A., and Brown, R. E. , "Novel Eulerian Vorticity Transport Wake Module for Rotrcraft Flow Analysis," *63rd Annual Forum of the American Helicopter Society*, Virginia Beach, VA, 2007.

[9]Nielsen, E. J., "Aerodynamic Design Optimization Using the Navier-Stokes Equations," *18th International Symposium on Mathematical Programming*, Copenhagen, Denmark, 2003.

[10]Wachspress, D. A., Quackenbush, T. R., and Boschitsch, A. H., "First-Principles Free-Vortex Wake Analysis for Helicopters and Tiltrotors," *59th Annual Forum of the American Helicopter Society*, Phoenix, AZ, 2003.

[11]Wachspress, D. A., Quackenbush, T. R., and Boschitsch, A. H., "Rotorcraft Interactional Aerodynamics with Fast Vortex/Fast Panel Methods", *Journal of American Helicopter Society*, Vol. 48 (4), 2003.

[12]Lynch, C. E., *Advanced CFD Methods for Wind Turbine Analysis*, Ph.D. thesis, Georgia Institute of Technology, 2010.

[13]O'Brien, D.M., *Analysis Of Computational Modeling Techniques For Complete Rotorcraft Configurations*, Ph.D. thesis, Georgia Institute of Technology, 2006.

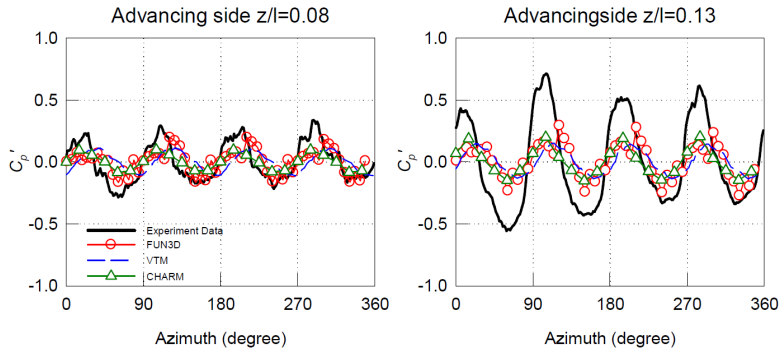

(a) Advancing side

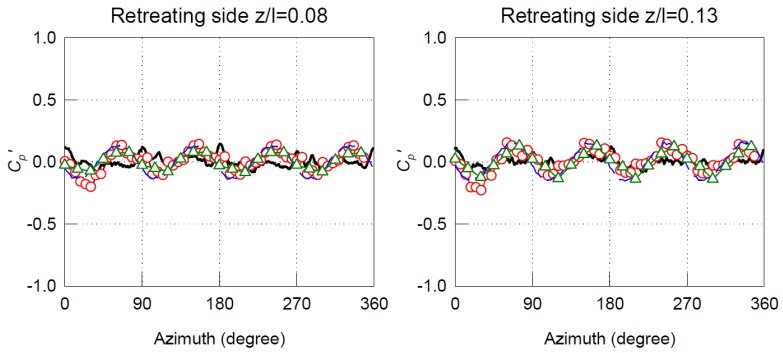

(b) Retreating side

Fig. 14: Unsteady pressure at various points around the fuselage at lengthwise location of $x/\ell = 0.9$, on the aft portion of the doghouse ($\mu = 0.23$, $C_T = 0.0064$). VTM data not available at $z/\ell = 0.08$ on the retreating side

[14]Abbott, I. H. and von Doenhoff, A. E., *Theory of Wing Sections*, Dover Publications, 1959.

[15]Anderson, J.D., Jr., *Aircraft Performance and Design*, McGraw-Hill, New York, NY, Anderson, J.D., Jr., 1999.

[16]Caradonna, F.X. and Tung, C., "Experimental and Analytical Studies of a Model Helicopter Rotor in Hover," NASA-TM-81232, USAAVRADCOM TR-81-A-23, 1981.

[17]Caradonna, F.X. and Tung, C., "Experimental and Analytical Studies of a Model Helicopter Rotor in Hover," *Vertica*, Vol. 5, 1981, pp. 149-161.

[18]Elliot, J.W., Althoff, S.L., and Sailey, R.H., "Inflow Measurements Made with a Laser Velocimeter on a Helicopter Model in Forward Flight. Volume I: Rectangular Planform Blades at an Advance Ratio of 0.15," NASA TM-100541, AVSCOM TM 88-B-004, 1988.

[19]Mineck, R.E. and Althoff Gorton, S.L., "Steady and Periodic Pressure Measurements on a Generic Helicopter Fuselage Model in the Presence of a Rotor," NASA TM-2000-210286, 2000.

[20]Freeman, C.E. and Mineck, R.E., "Fuselage Surface Pressure Measurements of a Helicopter Wind-Tunnel Model with a 3.15-Meter Diameter Single Rotor," NASA TM-80051, 1979.

[21]Smith, M.J., Shenoy, R., Kenyon, A.K., and Brown, R.E., "Vorticity Transport and Unstructured RANS Investigation of Rotor-Fuselage Interactions," Proceedings of the 35th European Rotorcraft Forum, Hamburg, Germany, September 2009.

[22]Kenyon, A.R. and Brown, R.E., "Wake Dynamics and Rotor - Fuselage Aerodynamic Interactions," Proceedings of the 63rd Annual Forum of the American Helicopter Society, Virginia Beach, VA, May 2007.

[23]Kenyon, A.R. and Brown, R.E., "Wake Dynamics and Rotor - Fuselage Aerodynamic Interactions," *Journal of American Helicopter Society*, Vol. 54 (1), 2009.

[24]Abras, J.N., Lynch, C.E., and Smith, M.J., "Advances in Rotorcraft Simulations with Unstructured CFD," Proceedings of the 63rd Annual Forum of the American Helicopter Society, Virginia Beach, VA, May 2007.

[25]O'Brien, D.M. and Smith, M.J., "Improvements in the Computational Modeling of Rotor/Fuselage Interactions Using Unstructured Grids," Proceedings of the 61st Annual Forum of the American Helicopter Society, Grapevine, TX, May 2005.

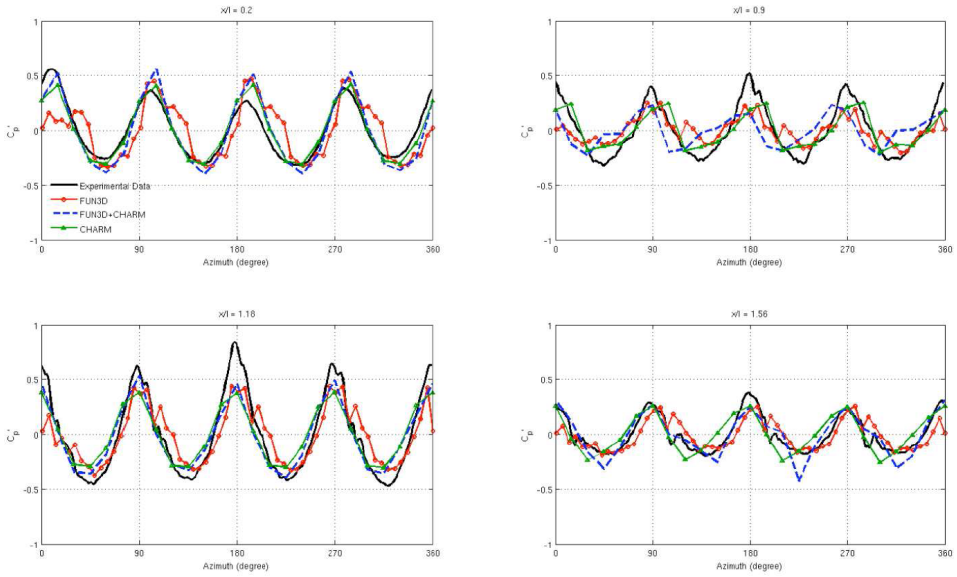

Fig. 15: Comparison of unsteady surface pressures along the ROBIN fuselage $\mu = 0.15$ predicted with FUN3D, FUN3D/CHARM and CHARM

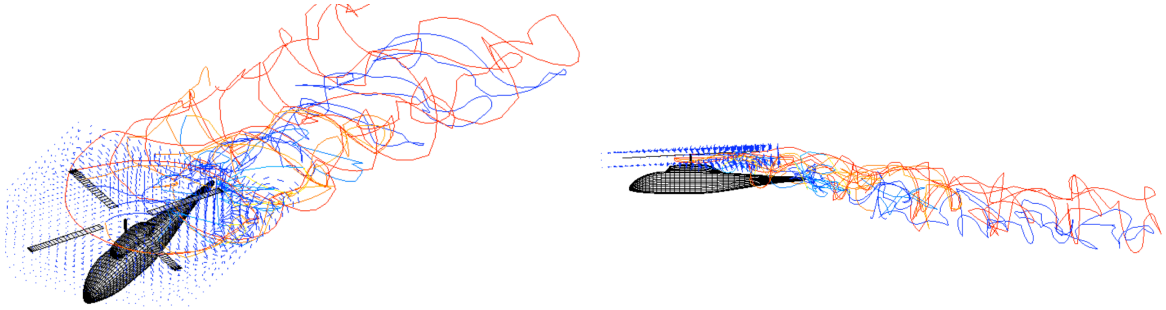

(a) Orthogonal view (b) Side view

Fig. 16: FUN3D/CHARM wake predictions for the $\mu = 0.15$ ROBIN case.

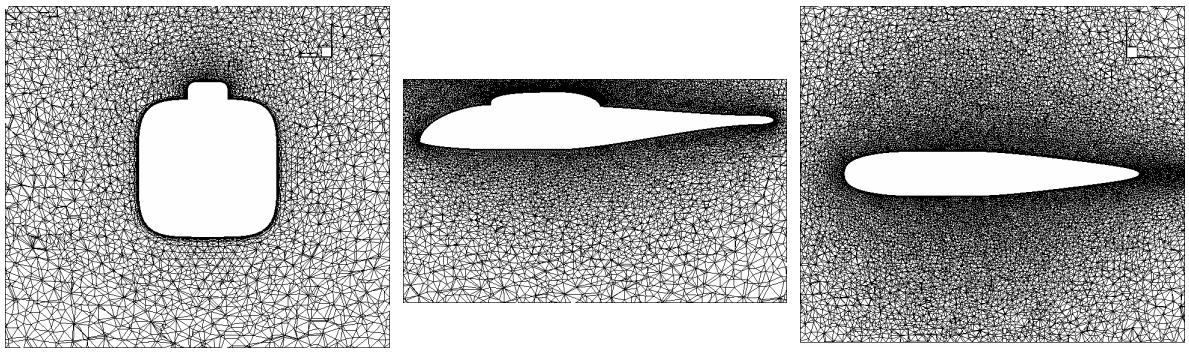

(a) Front view (b) Side view (c) Top view

Fig. 17: Close-up views of slices through the center of the body in the FUN3D fuselage grid.

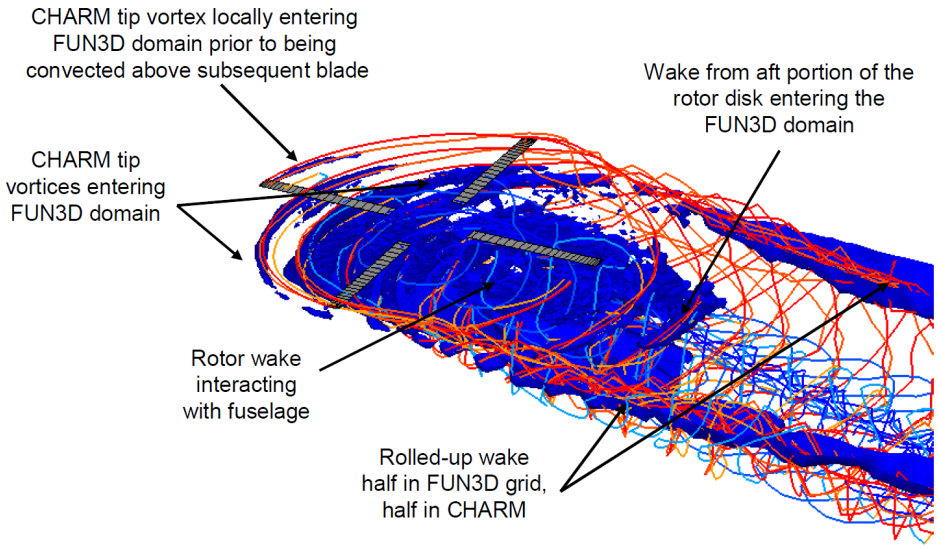

Fig. 18: 3D view of FUN3D/CHARM ROBIN calculation with CHARM rotor and wake coupled to a FUN3D fuselage.

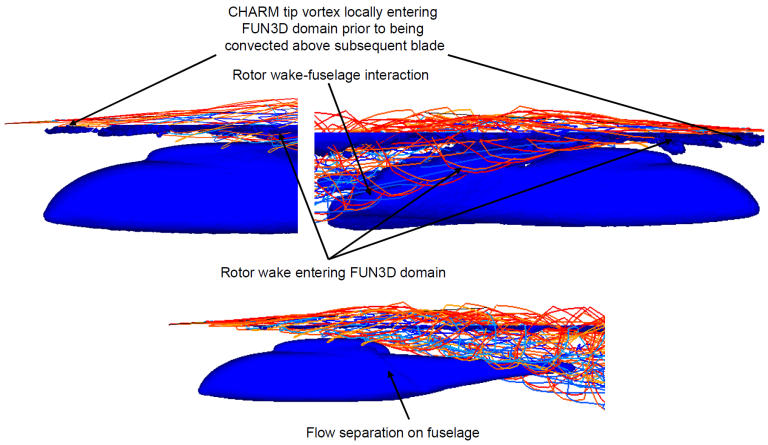

Fig. 19: Close-up views of the FUN3D/CHARM ROBIN predictions with CHARM rotor and wake coupled to a FUN3D fuselage. Front port side (upper left) and starboard side (upper right) showing wake entering the flow domain and port side (lower).

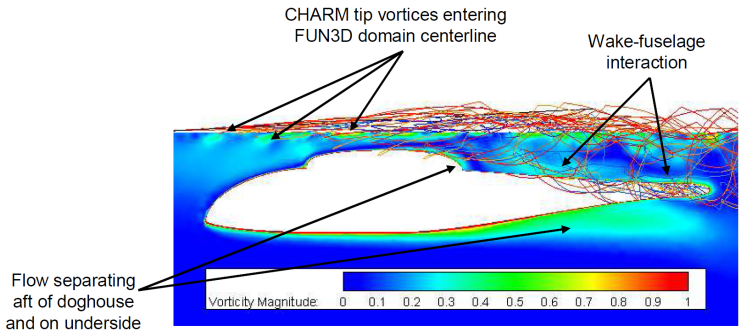

Fig. 20: 3D CHARM wake and contours of vorticity magnitude on a slice along the centerline of the fuselage.

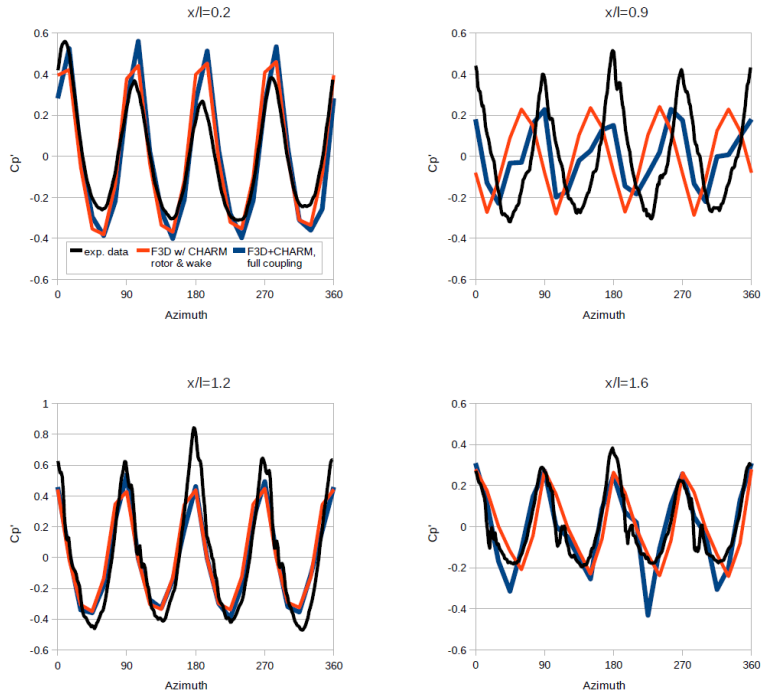

Fig. 21: Comparison of unsteady surface pressures along the ROBIN fuselage $\mu = 0.15$ predicted with FUN3D/CHARM. "F3D+CHARM full coupling" corresponds to FUN3D rotor and CHARM wake/fuselage, whereas "F3D w/CHARM rotor & wake" corresponds to the CHARM rotor wake model coupled to a FUN3D fuselage.